Chemical Engineering Journal 529 (2026) 172374

Contents lists available at ScienceDirect

Chemical Engineering Journal

journal homepage: www.elsevier.com/locate/cej

Electrodialysis with bipolar membranes for HCl and NaOH production: A scale-up analysis from the laboratory to a pilot-plant

Andrea Culcasi [a], Antonia Filingeri [a,b,*], Alessandro Tamburini [a], Giorgio Micale [a], Andrea Cipollina [a]

[a] Dipartimento di Ingegneria, Università degli studi di Palermo, Viale delle Scienze ed. 6, 90128, Palermo, Italy
[b] RESourSEAs SrL, Via Emanuele Notarbartolo 38, 90145, Palermo, Italy

ARTICLE INFO

Keywords:
Bipolar electrodialysis
Brine mining
Brine valorization
Electrodialytic water dissociation
Electro-membrane process
Water reuse

ABSTRACT

Electrodialysis with Bipolar Membranes (EDBM) is an electro-membrane process that produces acidic and alkaline solutions from salty water and electricity. In the available literature, this technology has been explored predominantly at the laboratory scale, with very few investigations at scaled-up levels.

This study investigated the effect of scale-up on the performance of the EDBM unit, comparing a laboratory-scale and a semi-industrial-scale unit under "scale-independent" equivalent operating conditions. Moreover, the experiments at both scales allowed the identification of scale-independent parameters governing the EDBM performance and, thus, enabled the assessment of key operational relationships. In this work, we propose a new methodology to find crucial scale-independent parameters and demonstrate the validity of the method through an original experimental campaign. As an application example, the effect of varying the initial solution volume ratios on process performance was systematically analyzed and confirmed across scales. Results indicate that the two units performed comparably, with less than 5 % difference typically observed between lab- and pilot-scale units in key parameters such as current density, voltage, and product concentrations, but also in key performance indicators. Doubling the volume of acid and salt solutions improved the systems performance, in terms of higher sodium hydroxide concentration, enhanced current efficiency, and reduced energy consumption. Indeed, at a OH^- concentration target of 0.5 mol L^{-1}, CE and SEC reached values of 86 % and 1.18 kWh kg^{-1}, respectively. A techno-economic analysis estimated a minimum production cost of 278 € ton_{NaOH}^{-1}. This work demonstrates that laboratory-scale experiments can reliably predict the behavior of upscaled systems and provides a solid basis for validating mathematical models, which can then be confidently used to simulate, optimize, and control larger-scale units.

1. Introduction

One of the greatest challenges of the present time is achieving sustainability in industry, but this is not attainable using conventional technologies. Indeed, in addition to having high energy consumption, most current technologies use resources identified as critical raw materials (CRMs) by the European Commission [1]. Two key examples of industry processes for which sustainability improvements are necessary are the production of acids, such as HCl, and bases, such as NaOH. HCl is typically produced either by direct synthesis from its elements or by reacting sodium chloride with sulfuric acid [2], while NaOH is typically a byproduct of the chlor-alkali process [3,4]. Often, these techniques produce very concentrated solutions of HCl (up to 12 mol L^{-1}) or solid NaOH pellets or powder to facilitate their transportation. In the water treatment applications, these products are then diluted with water to reach the desired concentration, but this process is extremely inefficient, as much of the energy used to concentrate the acid and base is then dissipated. Importantly, the Electrodialysis with Bipolar Membranes (EDBM) technology can be used to enhance the process efficiency [5], as it can produce acidic and alkaline solutions at the desired concentration directly [6], eliminating safety risk on transportation and handling concentrated reagents and the waste of energy mentioned above [7]. The effectiveness of this approach could be further enhanced if the chemicals were produced in-situ [6]. Indeed, in-situ production would not only eliminate the need to import chemical reagents, leading to economic savings, but also confer economic and environmental benefits by reducing the transportation of chemical products, which is energy-

* Corresponding author at: Dipartimento di Ingegneria, Università degli studi di Palermo, Viale delle Scienze ed. 6, 90128, Palermo, Italy.
E-mail addresses: antonella.filingeri@resourseas.com, antonia.filingeri@unipa.it (A. Filingeri).

https://doi.org/10.1016/j.cej.2025.172374
Received 27 September 2025; Received in revised form 20 December 2025; Accepted 27 December 2025
Available online 5 January 2026

Nomenclature

Acronyms

AEM	Anion Exchange Membrane
A-RED	Assisted-Reverse Electrodialysis
BPM	Bipolar Membrane
CEM	Cation Exchange Membrane
CRM	Critical raw material
ED	Electrodialysis
EDBM	Electrodialysis with Bipolar Membranes
EDTA	Ethylenediaminetetraacetic acid
ERS	Electrode rinse solution
IEM	Ion-exchange membrane
PE	Polyethylene
PI	Proportional-integral
RO	Reverse Osmosis

Symbols

A_m	Active membrane surface [m^2]
C	Solution concentration [mol L^{-1}]
CAPEX	Capital costs [€]
CE	Current efficiency [–]
F	Faraday constant [C mol^{-1}]
I	Current [A]
i	Current density [A m^{-2}]
LCoNaOH	Levelized cost of NaOH [€ ton^{-1}]
M	Mole weight [g mol^{-1}]
N	Number of triplets
OCV	Open Circuit Voltage [V]
OPEX	Operating costs [€ y^{-1}]
SEC	Specific energy consumption [kWh kg^{-1}_{NaOH}]
t	Time [h]
U	Voltage [V]
u	Channel flow velocity [cm s^{-1}]
V	Solution volume [L]
z	Ion valence

Subscripts and superscripts

Base	Base compartment
Lab	Laboratory unit
Pilot	Pilot unit
t	Generic time
triplet	Repetitive unit
0	Initial time

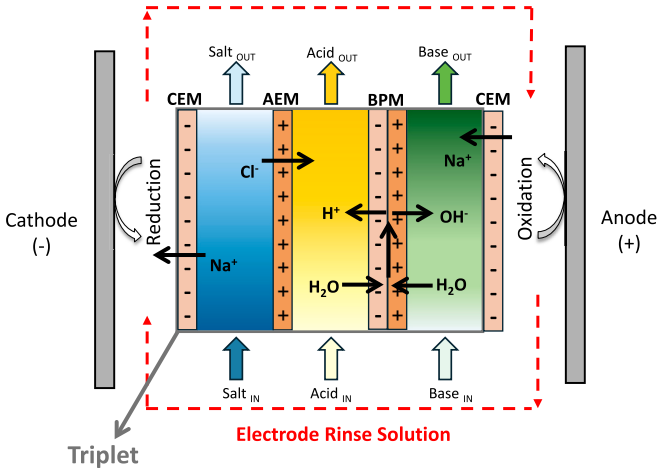

Fig. 1. Schematic representation of the EDBM process with a repeating unit, called triplet.

intensive and poses environmental risks [9].

EDBM is an electro-membrane process that allows the production of acid and alkaline solutions starting from a saline solution and using an external electric field, which acts as the driving force for water dissociation in the bipolar membrane interlayer and ion transport across the monopolar ion exchange membranes [10].

In particular, the EDBM unit comprises a stack of ion-exchange membranes (IEMs) and spacers, both made of polymers, placed between two electrodes [11]. The polymeric spacers create channels between the membranes to allow the flow of the electrolyte solutions (i.e., saline, acid, or alkaline) [12]. Furthermore, the electrodes (i.e., the cathode and the anode) can be made using graphite carbon source [13]. Therefore, the main components of the EDBM can be produced with non-critical raw materials according to the European Commission. EDBM utilises three types of IEMs: cationic (CEM), anionic (AEM) and bipolar (BPM) [1,13].

Conventional Electrodialysis for water desalination typically uses CEM and AEM to selectively transport ions, but the BPM plays a crucial role in the functioning of the EDBM technology. In fact, during the process, the BPMs facilitate the dissociation of water molecules into hydroxide ions and protons [10]. Concurrently, the salt ions in the saline solution move through the monopolar membranes in opposite directions based on their charge due to the application of the electric field, thus producing acidic and alkaline solutions (see Fig. 1).

Recently, EDBM has been proposed as a "circular driven" into treatment chains for the valorization of waste brines from desalination plants [15,16] or saltworks [17], with the aim of producing chemicals on-site, water [18–20], recovering critical raw materials such as magnesium, lithium, rubidium, and others. In this context, EDBM enables the in-situ production of the acidic and alkaline solutions used in these treatment chains [21]. Previous experimental studies on EDBM for producing HCl and NaOH solutions have been primarily conducted at the laboratory scale, with only a few studies focusing on scaled-up systems. Typical EDBM lab-units have active membrane areas between 0.0055 m^2 and 0.051 m^2, and total installed membrane areas of 0.03–1.53 m^2 [12,22–26]. Additionally, their experiments were typically conducted at a constant current density up to 1,000 A m^{-2} or a constant electric potential within the range of 9–35 V. Table 1 summarizes key EDBM studies reported for the production of HCl and NaOH.

In terms of EDBM stacks, several parameters influence unit performance. These include design aspects such as the active membrane area, current density, the channel dimension, initial solution volume or flowrates and the composition of the feed solutions. Particular emphasis should be placed on the selectivity and electrical behavior of the ion-exchange membranes, as these are key components in electrodialysis-related processes. Another relevant factor is the so-called "blank" resistance [34], which is directly related to the voltage drop associated with the electrode compartments (i.e., the blank potential). The blank resistance is a lumped parameter that includes the Nernst potential for the occurrence of the redox reactions, the overpotential related to the redox reactions, the ERS channel resistances, which is function of the spacer and the ERS solution characteristics, and the end membrane resistance. This voltage drop stems from the combined effect of the ohmic resistance and membrane potential of the end membranes, the ohmic drop across the electrode rinse solution, and, importantly, the anodic and cathodic reactions. However, this voltage drop becomes significant only in small-scale modules (i.e., stacks with a limited number of repeating units, typically between 1 and 10 [25,35–39]). In

Table 1
Summary of EDBM applications for the production of acids and bases from brines.

Process scale, active membrane area	Membrane	Feed composition[a]	Experimental conditions	Acid and base product concentrations	Current Efficiency	Specific Energy Consumption, SEC	Ref.
Lab-scale, 280 cm^2	WTS (AEM AR103N; CEM CR61N; BPM AR103N tr. and CR61N)	NaCl, 1.0–3.3 mol L^{-1}	300 A m^{-2}	1.2–1.4 mol L^{-1} NaOH <1.2 mol L^{-1} HCl	>60 %	1.4–1.8 kWh kg^{-1} NaOH	[11]
Lab-scale, 207 cm^2	Veolia Water Technologies and Solutions (CEM CR63TP; AEM AR103TP; BPM AR103N-BP and CR61N)	NaCl, 2.2–3.0 mol L^{-1}	400 and 600 A m^{-2}	0.9–1.8 mol L^{-1} HCl 1.0–2.1 mol L^{-1} NaOH	30–70 %	1.8–3.5 kWh kg^{-1} NaOH	[27]
Lab-scale, 7.1 cm^2	Astom *Co.* (AEM ASE, CEM CSE); Hefei Chemjoy Polymer Materials *Co.* Ltd. (AEM CJMA-4, CJMA-3; CEM CJMC-4, CJMC-3; BPM CJBPM-2)	NaCl, 1 mol L^{-1}	100 A m^{-2}	0.2–1.0 mol L^{-1} HCl 0.2–0.8 mol L^{-1} NaOH	61–83 %	2.2–3.1 kWh kg^{-1} NaOH	[28]
Lab-scale, 189 cm^2	Astom *Co.* (Neosepta® AEM AMX; CEM CMX; BP-1E o BP-1)	NaCl, 0.6 mol L^{-1}	9–13.5 V	1.9 mol L^{-1} HCl 2.0 mol L^{-1} NaOH	65 %	4 kWh kg^{-1} NaOH	[29]
Lab-scale, 55 cm^2	Astom *Co.* (Neosepta® CEM CMB; AEM AHA; BPM BP-1)	1.1 mol L^{-1} NaCl	25 V	1.8 mol L^{-1} NaOH	50 %	4.72 kWh kg^{-1} NaOH	[30]
Pilot-scale, 3200 cm^2	WTS (AEM AR103N; CEM CR61N; BPM AR103N tr. and CR61N)	1.0 mol L^{-1} NaCl	75 V o 200 A m^{-2}	0.5–1.0 mol L^{-1} HCl 0.5–1.0 mol L^{-1} NaOH	64–86 %	1.2–1.6 kWh kg^{-1} NaOH	[31]
Pilot-scale, 2500 cm^2	Hangzhou Lanran Technology *Co.*, Ltd. (AEM; CEM; BPM)	NaCl, 1.0–1.5 mol L^{-1}	500–700 A m^{-2}	0.8–3.4 mol L^{-1} HCl 1.0–3.3 mol L^{-1} NaOH	>54 %	1.5–2.3 kWh kg^{-1} NaOH	[32]
Pilot-scale, 1600 cm^2	Fumatech (Fumasep® AEM FAB-PK-130; CEM FKB-PK-130, FBM)	1.0 mol L^{-1} NaCl	200–500 A m^{-2}	0.9–1.0 mol L^{-1} HCl 1.0–1.1 mol L^{-1} NaOH	63–67 %	1.9–2.6 kWh kg^{-1} NaOH	[33]

[a] The reported feed composition refers to NaCl as the main salt for simplicity. Minor or trace species may also be present in the feed solution, but NaCl represents the dominant component.

such cases, the blank potential may account for a considerable fraction—greater than 25 % or more—of the total applied voltage. In larger modules, this contribution gradually represents a smaller percentage of the overall potential [5].

Moreover, electrode rinse solutions (ERSs) generally consist of a Na_2SO_4 solution [40] or an $FeCl_2/FeCl_3$ redox couple in an acidic medium, with the latter being used to prevent the precipitation of iron oxyhydroxides [26]. Notably, variations in the ERS composition have been shown to significantly affect the energy consumption in various studies [41], primarily due to differences in the electrodic reactions. Additional factors—such as the end-membrane resistance and the geometry of the electrode compartments—may also contribute to differences in the blank potential. However, despite the non-negligible effect of the blank potential in laboratory-scale units, in our previous experimental studies [11,26], we have specifically added thin platinum wires at the ends of the cell stack. These Pt wires were positioned to include only the repeating units of the EDBM stack, thereby not measuring the blank potential. This approach has also been adopted in other electromembrane processes, such as the Assisted-Reverse Electrodialysis (A-RED) [42].

Regarding experiments on pilot-scale systems, in a previous work [12], an EDBM unit (supplied by Fumatech®), featuring an active membrane area of 0.16 m^2 and a total area of 19.3 m^2, was investigated. This specific EDBM unit configuration included two internal stages with 20 triplets each. The solution enters one cell stack, flows through the channels, and is collected by an internal collector, which distributes it to the second cell stack. As a result, the two cell stacks are connected hydraulically in series and electrically in parallel. Although the membranes in this unit had previously been tested at the laboratory scale, an EDBM unit with this geometrical configuration had not, thus making direct comparisons with other laboratory-scale studies using the same membranes inappropriate. In another study, a WTS® EDBM plant was tested at the pilot scale [31]. For this, the tests were conducted with varying pressures in the channels in order to examine the effect of these changes on performance. The EDBM unit in this work used WTS membranes, had an active area of 0.32 m^2, and was equipped with a single cell stack with 50 triplets. Importantly, although similar membranes have been tested at the laboratory scale, these results cannot be compared to pilot-scale EDBM units with these membranes due to differences in the process conditions.

Demonstrating that results obtained at the laboratory scale can be effectively and reliably scaled up is crucial for minimizing the costs associated with the design, construction, and testing of pilot-scale plants, as well as for ensuring the efficient design of full-scale industrial facilities. However, the existing literature has largely overlooked the potential importance of identifying and analyzing scale-independent parameters, which are necessary for accurately comparing laboratory- and pilot-scale set-ups. Hopsort et al. [43] highlighted that scaling up Electrodialysis (ED) processes requires meticulous planning and optimization. As such, in order to scale up the ED process, they suggested the utilization of mathematical modeling, constant dimensionless numbers, and an appropriate specific surface area. However, the study did not provide information on the total installed area, the number of repeating units, or the channel length-to-width ratio, all of which are critical parameters for assessing the actual extent of axial concentration polarization (i.e., the ionic concentration gradient between the inlet and outlet). The spacer length-to-width ratio can significantly influence the occurrence of parasitic current phenomena, which reduce the useful cell current for a given applied external current [44,45]. Moreover, while this previous study suggests that ED systems can be scaled up by increasing the volume capacity, either by adding more repeating units or by operating multiple ED stacks in parallel, it does not explain how this volume scale-up can be effectively implemented. In another work [46], the authors aimed to scale up the Redox-mediated ED by increasing the number of i) electrodes, in order to increase the active area and electrodic reactions, and ii) channels, in order to operate with higher productivity, in the stacks. To the best of the authors' knowledge, no previous studies have investigated how the process time is affected by variations in parameters such as the volume of the external reservoirs (under batch mode), the total installed active membrane area, or the ratio between the electrolyte solution volumes. Similarly, the impact of the average fluid velocity in the channels has not yet been investigated as a relevant scale-up parameter in the existing literature.

Recognizing this critical gap relating to the scale-up of electromembrane processes, this study aims to establish a rigorous approach to identify and utilize scale-independent parameters, thus facilitating direct and meaningful comparison between different operational scales. Specifically, two EDBM stacks—one at the laboratory scale and one at

Table 2
Comparison of the geometric features of the stacks at laboratory and pilot scales.

	N [−]	Active membrane area [m^2]	Spacer			Dead volume [L]
			Width [cm]	Length [cm]	Thickness [μm]	
Lab-scale	5	0.023	2.6	75	760	0.18–0.22
Pilot-scale	50	0.32	18.9	178	760	25.8–28.5

the semi-industrial pilot scale—were rigorously compared under equivalent operating conditions and membrane configurations. Furthermore, batch experiments were conducted to investigate how variations in initial solution volumes impact the performance of the EDBM process during the valorization of waste brine into acid and base solutions. This research presents, for the first time, a clear methodological framework outlining how laboratory-scale EDBM experimental data can be systematically and reliably leveraged for scale-up and industrial design purposes. The approach introduced herein offers practical guidance on collecting essential performance data at the laboratory scale that can be employed to design larger-scale plants. Such a process would reduce the risks and costs involved in transitioning to pilot- and industrial-scale implementations.

2. Materials and methods

This section describes the experimental setups for both laboratory- and pilot-scale, the experimental procedures, the analytical techniques, and the determination of the scale-independent parameters related to the experiments performed with the two EDBM units.

2.1. Experimental setup

Both the small-scale laboratory unit (referred to as the lab-scale unit in this work) and the larger semi-industrial system (referred to as the pilot plant in this work) were provided by WTS and had the same membranes. Specifically, the triplets are composed of WTS commercial IEMs: anionic (AR103N), cationic (CR61N), and bipolar, with the latter obtained by overlapping the cationic (CR61N) membrane and a treated anionic (AR103N tr.) membrane.

The spacers are made of woven polypropylene net 760 μm thick. The gaskets in the pilot plant form a U-shaped fluid path with a length of 1.78 m, whereas those in the lab-scale unit form an S-shaped fluid path with a length of 0.75 m.

Each EDBM unit in both systems comprises two electrodes made of stainless steel (the cathode) and platinum-plated titanium (the anode).

Diluted solutions at 0.05 mol L^{-1} of acid and alkaline reactant and synthetic NaCl solutions are used to feed the stacks. The units are specifically designed so that the alkaline solution feeds both the alkaline and the electrode compartments (i.e., the anolyte and catholyte). As a result, the units have three distributors and three collector manifolds. This configuration has not been explored in previous studies on EDBM units, as such units generally include a fourth compartment used for the Electrode Rinse Solution (ERS). Therefore, the electrodic reactions primarily consist of hydrogen evolution at the cathode and oxygen evolution at the anode. Additionally, the electrode channels in these units are assembled with two spacers, as this makes it easier to remove bubbles.

At the end of each test at both dimensional scales, washing procedures with softened or demineralized water were carried out to preserve the integrity of the ion-exchange membranes and to prevent fouling

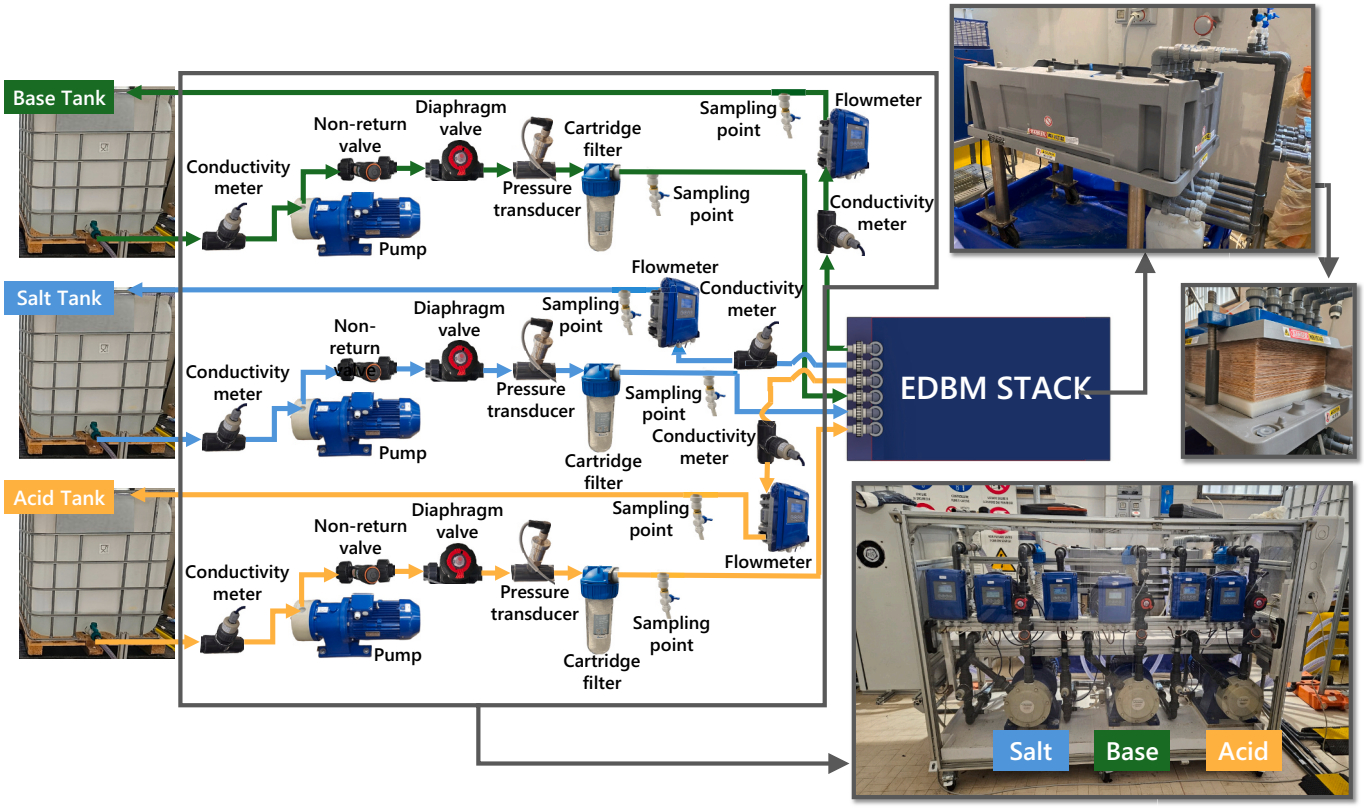

Fig. 2. Schematic representation of the hydraulic circuits and some pictures of the real pilot stack and equipment.

phenomena. The experimental campaigns were carried out at ambient temperature. The laboratory- and pilot-scale stacks were operated at the same mean channel flow velocity.

A size comparison of the two EDBM units is shown in Table 2. The specific characteristics of each system (i.e., the lab-scale unit and the pilot plant) are further discussed in the following sub-sections.

2.1.1. Lab-scale unit

The laboratory-scale unit is an Electromat MkI ED STACK (WTS). The unit includes 5 triplets and has an active electrode area of 0.023 m^2. The system comprises three identical hydraulic circuits, which are made up of polyethylene (PE) fittings, valves and tubes. For the experiments, three plastic containers were utilized, each with a maximum capacity of 2–5 L. The measured dead volume for the three hydraulic circuits was 180–220 mL. Samples were taken using syringes approximately every 30 min. Pressure gauges are installed at the inlet of the EDBM stack. The mass of the solutions is determined using precision scales (KERN KB, with a maximum capacity of 10,000 g and a precision of 0.1 g). The mean channel flow velocity was set to 5 cm s^{-1}.

The solutions flow to the EDBM stack through peristaltic pumps (LeadFluid, models BT601S and YT15 head). The electrical power for the stack is supplied by a precision (B&K, model 1902B) power supply. Finally, voltage and current measurements are taken using two bench multimeters (Fluke, model 175). One multimeter is connected to the EDBM unit in parallel for the voltage measurements, and the other multimeter is connected in series to measure the electric current. Platinum wires (Alfa Aesar Pt wires, 0.127 mm diam. hard, 99.9 % metal basis) were inserted in the ERS compartments when assembling the stack in order to measure the fraction of the stack voltage that was applied to the five triplets, thus excluding the voltage drop at the electrode.

2.1.2. Semi-industrial pilot

A WTS ED-STACK, 3CBPED module, was chosen for EDBM pilot unit. The unit comprises a set of membranes and spacers with 50 triplets. The electrodes have an active area of 0.32 m^2, and the total active membrane area is 48 m^2.

Three identical hydraulic circuits are present to flow through the EDBM. The measured dead volume for the three hydraulic circuits was determined to be 25.8–28.5 L and considered during the post-processing phase of the data analysis, specifically for the calculation of the performance indicators.

2.1.2.1. Hydraulic circuits, sensors and main electric components. The hydraulic circuits including valves, fittings, and probes schematically represented in Fig. 2 along with some pictures of the real pilot stack and the relevant equipment.

The pilot incorporates three pumps (TEOREMA PTM®) for the acid, base, and saline solutions. To ensure the appropriate fluid-dynamic conditions in the EDBM unit, it was operated with an average flow velocity in the channels $\sim$ 5 cm s^{-1}, which corresponds to a volumetric flow rate range of 25 L min^{-1}.

As a safety precaution, cartridge filters (ATLAS®) were installed to prevent fouling of membranes and spacers in the stack.

Magnetic flowmeters (OPTIFLUX 4100, KROHNE®) were installed to measure the stack outlet flow rates, and pressure transducers (OPTIBAR P 1010C, KROHNE®) were installed at the stack inlet to assess pressure drops along the hydraulic circuit. Conductivity and temperature sensors (OPTISENS IND 1000, KROHNE®) are used to monitor the conductivities and temperatures of the solutions, respectively. The data acquisition hardware includes a chassis with acquisition and command boards (National Instruments®). The pilot plant is monitored and controlled using the National Instruments LabVIEW® software. The EDBM stack is powered by a DC drive with a maximum output of 17.5 kW (GIUSSANI Srl).

2.1.2.2. Solution tanks. The system includes six separate IBC tanks, each with a maximum volume of 1 m^3, to enable the EDBM to operate in various process modes (refer to the "Operating modes" section). These tanks were calibrated to facilitate the visual determination of the solution volume with a resolution of 10 L. The liquid volume was recorded manually each time a sample was taken. The storage tanks are located indoors, and the containers holding the acid and alkaline solutions are each connected to external forced ventilation via an aerator. The laboratory housing the system is also equipped with extra window fans to ensure continuous air exchange. Each of the six tanks is placed on one of three containment basins, with two tanks per basin. These basins are designed to hold the full volume of the containers above in case of leakages.

2.1.2.3. Operating modes. The EDBM pilot unit was operated in batch closed-loop configuration, i.e., recirculating solutions of the same type within their tank until a certain target concentration is reached. Moreover, other operational modes were specifically designed for draining the containers, cleaning the stack and hydraulic circuits, and refilling the containers with softened water. The implementation of these extra modes is facilitated by a valve system.

2.1.2.4. Acquisition and control system. A purposely designed acquisition and control system was programmed using the LabVIEW software to: i) acquire the signals from the sensors and ii) control the flow rates and the pressures of the three main solutions. Standard proportional-integral (PI) feedback controllers were designed for these purposes. The gain and time constants of the controllers were initially calculated using empirical correlations [47,48]. Lastly, the controller parameters were fine-tuned.

2.2. Solution preparation

The pilot- and lab-scale experiments were performed with synthetic solutions prepared with softened and demineralized water, respectively. The magnesium and calcium content of the softened water was estimated by ethylenediaminetetraacetic acid (EDTA) complexometric titration in order to ensure that the solutions were prepared using water with a maximum Ca and Mg concentration of 10 ppm of $CaCO_3$ equivalent. This hardness limit was suggested by the membrane manufacturer in order to avoid damage to the membranes.

The saline solution was prepared with NaCl (>99.5 % purity, Saline di Volterra s.r.l., Italy) at a concentration of 1.0 mol L^{-1} to mimic the concentration of brine from Reverse Osmosis (RO) or saltworks. The acid and base solutions were prepared at an initial concentration of 0.05 mol L^{-1} with a concentrated solution of HCl (ACS Reagent 37 %, Honeywell, Fluka) and solid micropearls of NaOH (technical grade, Inovyn), respectively. Low-concentration acids and bases were utilized to start the tests as an alternative to water to prevent excessively high electrical solution resistance in the channels in the initial phase of the test.

2.3. Experimental procedure and analytical technique

Leakage tests were performed on both laboratory- and pilot-scale units operating in a closed-loop configuration without applying any electrical potential. Softened or deionized water was recirculated through all compartments for 5 h in the pilot-scale unit and 1 h in the laboratory-scale unit to quantify leakage rates. In both stacks, the leakage percentage was found to be below 5 % per hour, defined as the ratio between the mass variation and the initial solution mass.

Before starting the experiment, at the laboratory scale, the solutions were fed to the empty stack, whereas at the pilot scale, the solutions were fed in open-loop to replace the storage solution in the stack.

Before applying the electric current, the Open Circuit Voltage (OCV) was measured using a multimeter connected to the electrodes. The

initial phase of the test was conducted under potentiostatic conditions to prevent an increase in the voltage resulting from the low concentration of the initial acid and base solutions, resulting in elevated channel resistances, if fixed current was applied. A fixed voltage of 1.5 V per triplet was applied at the platinum wires in order to ensure a similar initial current density to the pilot scale. As a result, the total applied voltage for the pilot EDBM stack was 75 V. In this initial phase of the test, the corresponding electric current increased over time due to the reduction in the internal stack resistance, which was caused by the production of acid and base. Upon reaching a current density of 200 A m^{-2} (65 A at the pilot scale and 4.52 A at the laboratory scale), the test was shifted to galvanostatic conditions. In the second phase of the test, if the corresponding voltage reached the maximum limit (i.e., 75 V and ~ 12.6 V at pilot and lab-scale, respectively), the control system was switched again to the potentiostatic mode.

Samples were periodically collected from the inlet streams. The sampling volumes were ~ 50 mL and ~ 4 mL for the pilot- and lab-scale units, respectively.

Throughout the test period, this sampling procedure was conducted at approximately 30–60 min intervals for both the pilot plant and the lab-scale unit. The collected samples were analyzed using titration to ascertain the concentration of protons and hydroxide ions, as well as through chromatographic analysis to assess other ions concentration. Titrations were carried out manually with standard solutions of 0.1 mol L^{-1} HCl and 0.05 mol L^{-1} Na_2CO_3 for the base and acid samples, respectively, and a 0.1 % w/w Methyl Orange solution (ACS dye content 85 % w/w, SIGMA-ALDRICH) was used as a visual pH indicator. Ion chromatographic analyses were carried out to estimate concentration of the other ions (i.e., Na^+ and Cl^-) in the three solutions. The Ion Chromatograph was a Metrohm 882 compact IC plus with anion (Metrosep A Supp 5–250/4.0) and cation (Metrosep C 6–250/4.0) columns. The mobile phases of the anion and cation columns of the chromatograph were a mixture of 4.5 mmol L^{-1} HNO_3 and 0.5 mmol L^{-1} $H_2C_2O_4$ and a mixture of 3.2 mmol L^{-1} Na_2CO_3 and 1.0 mmol L^{-1} $NaHCO_3$, respectively.

2.4. Experimental campaign

The primary goal of this work is to conduct a rigorous scale-up analysis and develop a robust methodology for identifying scale-independent parameters for EDBM, i.e., process variables that, regardless of the system's dimensional scale, fully determine its behavior. These parameters will facilitate accurate and reliable comparisons between different scales, ultimately guiding the scale-up process from laboratory-scale experiments to industrial-scale EDBM units. Indeed, using such parameters, multiple units could run under “equivalent” operating conditions regardless of their size.

Specifically, from the process variables, four corresponding scale-independent parameters were identified: i) current density, ii) voltage per triplet, iii) mean channel flow velocity, and iv) test duration. Electrical parameters such as the current density (i) and voltage per triplet (ii) determine the unit's electrical behavior (i.e., the ionic fluxes across the IEMs), whereas under the same applied electrical conditions, the mean channel flow velocity (iii) and the test duration (iv) govern the actual product concentrations. At fixed initial concentrations of the streams, the EDBM process would not be expected to behave differently at the two scales, unless due to the influence of other non-ideal phenomena such as differences in membrane aging or unexpected equipment damage unrelated to the scale-up. Firstly, current density represents the flux of electrons crossing the active membrane area, and this parameter must be kept constant to ensure equivalent operating conditions. Indeed, when using the same current density, two systems with different active membrane areas would have different current intensities (i.e., the corresponding process variable). Secondly, the voltage per triplet refers to the average potential difference established across each triplet and is also a scale-independent parameter, particularly when the physicochemical properties of the membranes are the same (e.g., in terms of the areal resistance). The associated process variable is the total electric potential difference applied to the EDBM stack by an external power supply. Additionally, the voltage per triplet affects the energy consumed by the process (i.e., the SEC, see Section 2.5). It is worth noting that the voltage drop at the electrode chambers would be negligible in a pilot plant with 50 triplets, but it may represent up to 30 % of the voltage applied to the EDBM stack in a lab-scale unit. Therefore, in lab-scale units, it is important to exclude the electrodic voltage drop from the total applied using platinum wires placed in the unit. Thirdly, the mean channel flow velocity is another scale-independent parameter, for which the corresponding process variable is the volumetric flow rate through the EDBM unit. Specifically, since the spacers used at the lab- and pilot-scales have the same mesh, once this velocity is fixed, its effect on both the axial polarization (i.e., the concentration gradient along the flow direction) and radial polarization will remain comparable. Moreover, the identical mean channel flow velocities, equal channel thicknesses, and similar electrolyte densities and viscosities ensured that both the lab- and pilot-scale stacks operated under comparable Reynolds numbers. As discussed in the introduction, the spacer length-to-width ratio can significantly affect the extent of parasitic current phenomena. As such, in this study, experiments were conducted with a high spacer length-to-width ratio at both scales.

Table 3
List of process variables and the associated scale-independent variables.

Lab-scale process variable	Scale-independent parameters	Pilot-scale process variables
Current intensity, I_{lab}	Current density, i	Current intensity, I_{pilot}
Applied voltage, U_{lab}	Triplet voltage, $U_{triplet}$	Applied voltage, U_{pilot}
Solution flowrate, Q_{lab}	Channel velocity, u	Solution flowrate, Q_{pilot}
Solution volume, V_{lab}	Test time, t	Solution volume, V_{pilot}

Finally, the normalized time is a scale-independent parameter that accounts for differences in both the total installed active area and the initial volumes for the acid, alkaline, and saline solutions. Specifically, these initial solution volumes represent the process variable, and this variable can be scaled according to the total membrane area. The volume of the electrolyte solutions in the external containers for the pilot plant was determined by scaling up the initial volume in the lab-scale unit tanks using the following equation:

$$V_{pilot} = V_{lab} \cdot \frac{N_{pilot} \cdot A_{m,pilot}}{N_{lab} \cdot A_{m,lab}} \quad (1)$$

where V_{lab} and V_{pilot} are the volumes at the laboratory- and pilot-scale, respectively; N_{lab} and $A_{m,lab}$ are the number of triplets and the active membrane area of the lab-scale unit; and N_{pilot} and $A_{m,pilot}$ are the number of triplets and the active membrane area of the pilot-scale unit. The use of this correlation when determining the initial solution volumes, together with the other independent parameters, allowed for the comparison of the base and acid concentrations at the lab- and pilot-scales at equivalent timepoints. Furthermore, scaling the volumes as described in Eq. 1 also results in equal process specific charges (Ah L^{-1}). This equivalence across dimensional scales is demonstrated in the Supplementary Material. The scale-independent parameters and their associated process variables are summarized in Table 3. A prerequisite for using these parameters to compare between scales is all of the solutions having the same initial concentrations. Furthermore, using the present methodology, results from lab-scale plants can be applied to the pilot scale if using the same types of membranes. Otherwise, these differences must be taken into account, which was beyond the scope of this work.

It is important to note that the dead volumes of hydraulic circuits implemented at the different scales may vary significantly. Specifically, dead volume refers to the volume of solution contained within the hydraulic circuit, including the volume in the components such as the

Table 4
List of the experiments carried out with the laboratory and pilot units.

# Code	Pilot[a]			Laboratory[a]		
	V_{salt}	V_{base}	V_{acid}	V_{salt}	V_{base}	V_{acid}
S2_B1_A1	500	250	250	3.50	1.75	1.75
S2_B2_A1	500	500	250	3.50	3.5	1.75
S2_B1_A2	500	250	500	3.50	1.75	3.50
S1_B1_A1	250	250	250	1.75	1.75	1.75
S2_B2_A2	500	500	500	3.50	3.50	3.50

[a] Tests carried out with pilot and laboratory units will be identified in the code by the letter "P" and "L", respectively.

valves, the filters, and the EDBM unit itself. Therefore, the dead volume at both scales being compared should be estimated and taken into account. Importantly, despite the significant difference in the absolute dead volumes between the lab- and pilot-scales, their relative proportion compared to the initial solution volumes were comparable (i.e., approximately 5–10 %), resulting in a similar impact of the dead volume across scales.

At the beginning, the tanks contained the volumes shown in Table 4, which summarizes the operating conditions of the experimental campaign. The initial volumes varied from 250 L to 500 L at the pilot-scale and from 1.75 L to 3.5 L at the laboratory scale. The effectiveness of the method used to identify scale-independent parameters was validated by comparing the performance of both the lab- and pilot-scale units. Specifically, the impact of varying the initial volumes of acid, base, and salt on EDBM performance was investigated at both scales.

Several tests were repeated at both the lab- and pilot-scales to assess the experimental deviations. Very good repeatability was observed, with average deviations of 4.4 % and 4.7 % for the lab- and pilot-scales, respectively. Error bars have been included for all of the trends in process variables described in the manuscript.

2.5. Calculation of key performance indicators

The experimental data was processed to obtain the key performance indicators for the EDBM units. Specifically, the following indicators were considered:

Current efficiency, CE (–) is the fraction of the electrical charge input into the EDBM that is effectively converted into OH^- ions, as shown in Eq. (2):

$$CE = \frac{\left(C_{OH^-,t} \cdot V_{base,t} - C_{OH^-,0} \cdot V_{base,0}\right) \cdot z\, F}{N \cdot 3,600 \cdot \int_0^t I\, dt} \quad (2)$$

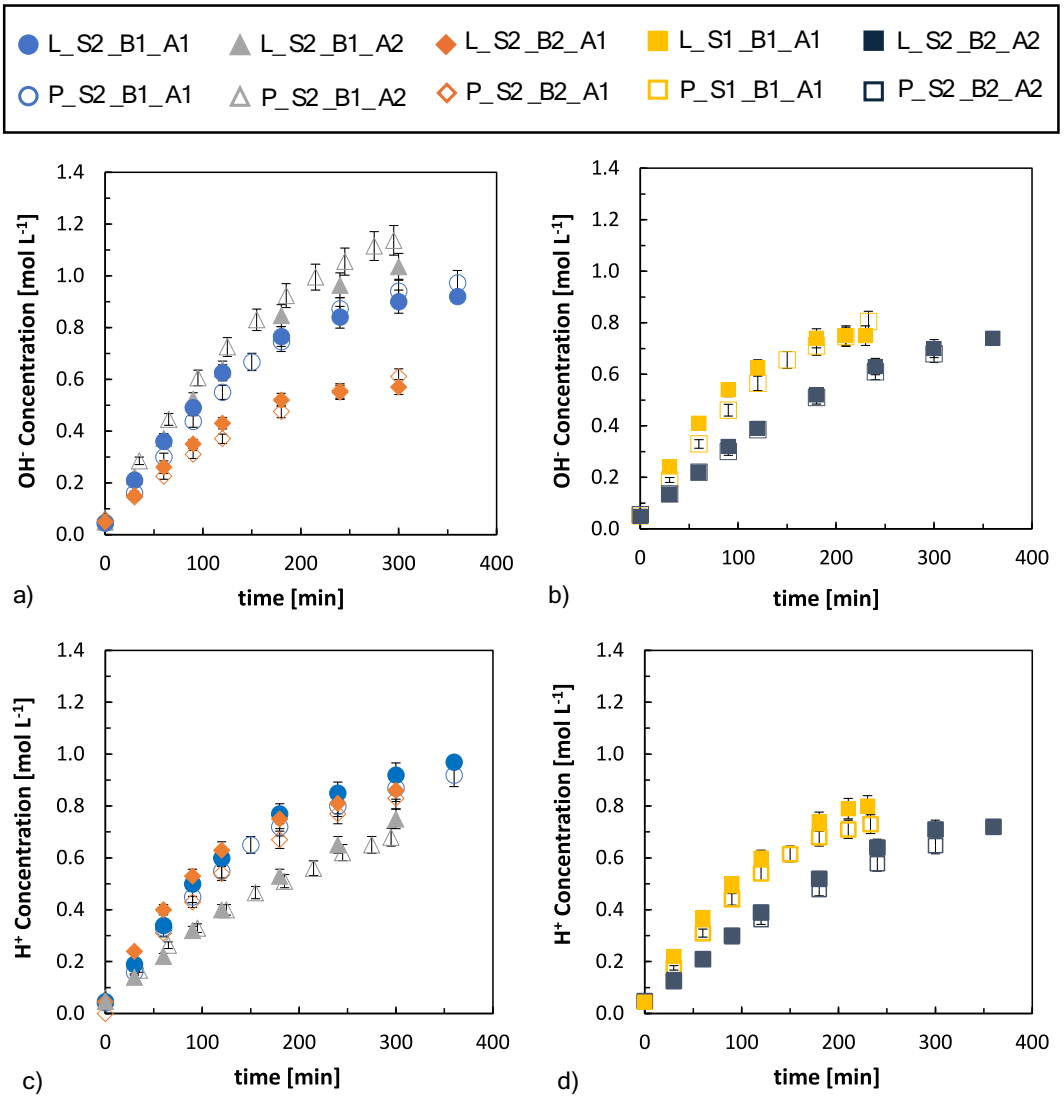

Fig. 3. Concentration profiles over time for tests carried out at both the pilot and laboratory scales under different scenarios for a) and b) OH^- concentration and c) and d) H^+ concentration. a) and c) refer to tests with different initial volumes while b) and d) report tests with the same initial volumes.

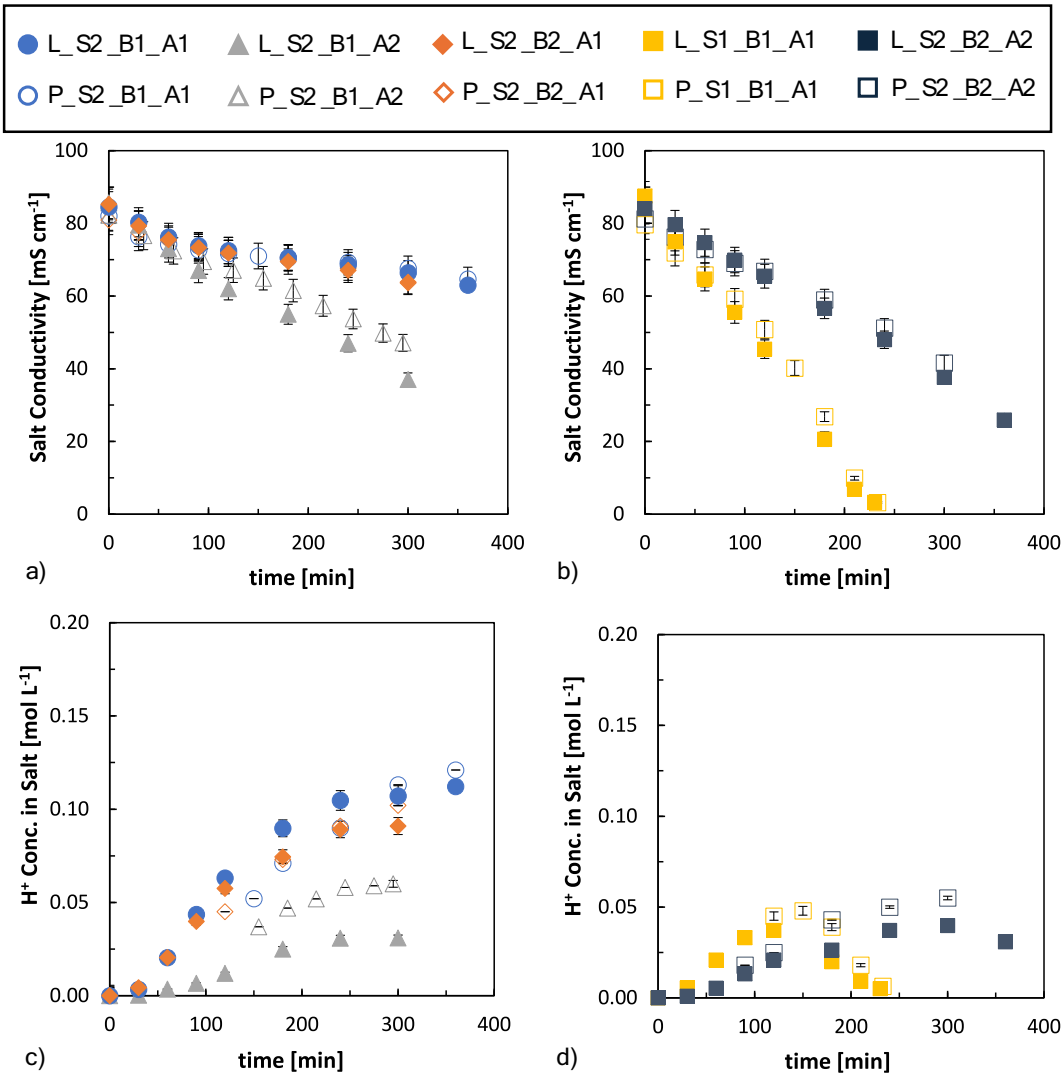

Fig. 4. Conductivity profiles (a) and (b) and H^+ concentration (c) and (d) profiles of the salt compartment over time for the tests conducted at both pilot and laboratory scales for all the scenarios investigated. a) and c) refer to tests with different initial volumes while b) and d) report tests with the same initial volumes.

where $C_{OH^-,t}$ is the concentrations of OH^- ions (mol L^{-1}) at the generic time t (h) and $C_{OH^-,0}$ is the OH^- concentration at the beginning of the test, respectively, $V_{base,t}$ (L) is the base solution volumes at the generic time t and $V_{base,0}$ (L) is the base solution volumes at the beginning of the test respectively. Specifically, the two volumes included both the solution volume in the tank and the dead volume in the rest of the hydraulic circuit (including the stack). I (A) is the electric current intensity.

Specific Energy Consumption, SEC (kWh kg^{-1}), is the energy used by the EDBM unit to produce 1 kg of NaOH. It is defined as follows:

$$SEC = \frac{\int_0^t U{\cdot}I\,dt}{\left(C_{OH^-,t}{\cdot}V_{base,t} - C_{OH^-,0}{\cdot}V_{base,0}\right){\cdot}M_{NaOH}} \quad (3)$$

where U is the electric potential and M_{NaOH} is the NaOH mole mass (g mol^{-1}).

3. Results and discussion

This section describes the experimental results obtained at the lab- and pilot-scales when operating the two units under "equivalent" operating conditions, as described in Section 2.4. A comparison between the lab- and pilot-scales was carried out to identify performance variations when operating with the same scale-independent parameters.

3.1. Acid and base concentrations and salt conductivity trends

Fig. 3 shows the trend in the OH^- and H^+ concentrations over time for all five investigated scenarios, considering both the laboratory-scale and pilot-scale experiments.

When operating the two units (i.e., the laboratory and pilot scale units) under equivalent conditions and, thus, the same scale-independent parameters, the OH^- concentration initially increased linearly and then tended to plateau. At high concentrations, the rate of increase became progressively lower over time, despite the fixed current density, due to the growing impact of detrimental phenomena, such as acid and base diffusion. When operating with equivalent scale-independent parameters (as shown in Table 3), the relative extent of detrimental phenomena was similar between the laboratory and pilot-scale tests.

Additionally, at both scales, the highest base concentrations were achieved when the initial volumes of the acid and saline compartments were twice that of the base compartment (i.e., scenario S2_B1_A2). This finding occurred because the lower H^+ concentration (as shown in the Fig. 3c) in the acid compartment during the test reduced the proton concentration gradient between the acid and base compartments, thereby mitigating the impact of diffusive and neutralization phenomena. The decrease in undesired phenomena was confirmed by the fact

that when doubling the acid volume in test S2_B1_A2, the H^+ concentration reached values larger than a half of the concentration of test at S2_B1_A1 (i.e., doubling the volume of the acidic solution leads to an increase in current efficiency). Conversely, the lowest OH^- concentration was observed when the initial volume of the alkaline solution was doubled. In this case, the reduced OH^- concentration had a minor impact on the acid concentration, resulting in similar H^+ concentrations for both tests, S2_B2_A1 and S2_B1_A1. This difference in behavior can be attributed to the distinct ion mobilities of protons and hydroxide ions across the membranes. Importantly, this behavior of the membranes is independent of the system scale.

In particular, diffusion phenomena occurred across both the monopolar and bipolar membranes, thus leading to an increase in Na^+ and Cl^- concentrations in the acid and alkaline compartments. As a result, similar trends were observed across the scenarios in terms of the acid and base purities. Indeed, changing the volume ratio affected the concentrations of protons, hydroxide, and other ions proportionally. The final purities were 91.5 % ± 3.9 % for the acid and 94.1 % ± 3.4 % for the base. The sodium and chloride ion impurities found in the acid and base products, respectively, during the present experimental campaign are consistent with those observed in a previous laboratory-scale study (i.e., approximately 8 % impurities in the acid product and 3 % in the base product) [24].

Therefore, using the same EDBM stack and under comparable electric current conditions, it is possible to adjust the solution volumes in batch operation to obtain acidic and alkaline products with higher or lower concentrations regardless of the unit scale. This principle also applies to continuous operation, where the volume ratio should be replaced by the ratio of the volumetric flow rates of the solutions fed into the unit, as in open-loop or feed-and-bleed configurations.

In scenarios where the initial solution volumes were equal among the acid, base, and saline compartments (i.e., S1_B1_A1 and S2_B2_A2), the final concentration of H^+ in the acid and the OH^- in the base did not depend on the solution volume used. Indeed, in these scenarios, the only factor that changes is the time required to reach a specific product concentration. Therefore, the solution volume (when the volume is the same in the three compartments) does not significantly impact unit performance (e.g., in terms of current efficiency), whereas the ratio between solution volumes plays a key role in determining system behavior.

Similarly, in these scenarios, the concentrations of Na^+ and Cl^- ions in the acid and base solutions were not significantly influenced by the solution volumes. Indeed, the final Na^+ and Cl^- concentrations observed in the two tests performed with identical initial volumes were very similar. This result suggests that the extent of diffusive fluxes or co-ion migration across the membranes remains globally comparable when targeting the same final concentrations of acid and base products.

Moving on to the saline solution, Fig. 4a and b show the conductivity profiles over time for the laboratory and pilot-scale experiments.

The saline solution conductivity decreased over time, with similar trends in both the laboratory and pilot-scale experiments when using the same scale-independent parameters, as was observed for the acid and base solutions.

At both scales, the conductivity of the saline solution depends on the sodium (Na^+), chlorides (Cl^-) and protons (H^+) concentrations. Indeed, although the saline channel is bordered on one side by the acid channel and on the other by the alkaline channel, the greater diffusion of HCl compared to the NaOH into the saline compartment results in net acidification.

In tests where the solution volumes were imbalanced (see Fig. 4c), the concentration of H^+ in the salt channel consistently increased over time during the initial phase of the experiment, approaching a plateau once the acid concentration in the acid channel stopped increasing. As observed in our previous paper [11], Na^+ initially exhibits a higher transport number across the CEM. During the test, as the OH^- concentration in the alkaline compartment increases, the CEM cannot completely block hydroxyl ions, which are partially transported across the CEM from the base to the salt channel. Consequently, over time, the transport number of OH^- increases at the expense of Na^+ transport. In the early stages of the test, the contribution of H^+ transport remains negligible. Doubling the acid volume reduced the proton concentration in the acid channel, thus decreasing proton transport to the salt solution. The lower proton concentration favored sodium ion migration from the saline to the base compartment. Indeed, transport numbers are directly linked to species concentrations, meaning proton transport was comparatively lower in this case. Conversely, in scenarios where the initial volumes are balanced (see Fig. 4d), sodium migration prevails over the undesired transport of OH^- only in the early stages of the experiment, and the H^+ concentration in the salt solution increases similarly to scenarios with imbalanced volumes. However, during the test, the concentration of sodium reduced significantly, reaching a final value of 0.01 mol L^{-1} and 0.26 mol L^{-1} for S1_B1_A1 and S2_B2_A2, respectively, due to the lower initial available moles for test S1_B1_A1 or the larger Na^+ transport towards the base for test S2_B2_A2. Notably, the difference between the final concentrations (i.e., 0.01 mol L^{-1} versus 0.26 mol L^{-1}) was primarily due to the duration of test S2_B2_A2 being less than half of S1_B1_A1.

Once the sodium concentration in the saline compartment reaches a critical low threshold, the H^+ ions in the salt become competitive with the Na^+ ions in terms of migration towards the alkaline channel. Therefore, the proton migration from the salt channel towards the alkaline channel becomes significant enough to reverse the proton concentration trend in the salt channel from increasing to decreasing. This critical transition occurs abruptly (Fig. 4d), marking the point at which the remaining Na^+ begin competing with H^+ ions in the salt channel, resulting in the transport of both ions across the CEM towards the base channel. The operational mode following this transition is particularly noteworthy, as it partially limits the increase in OH^- concentration in the alkaline solutions. Despite differences in test duration due to varying initial volumes, the proton concentration in the salt channel for both the S2_B2_A2 and S1_B1_A1 experiments—at both pilot and laboratory scales—reached a similar maximum before decreasing when the saline conductivity approached approximately 37–40 mS cm^{-1} and the Na^+/H^+ ratio dropped below 13.

There was significant proton migration despite Na^+ having a higher concentration than H^+ (< 0.06 mol L^{-1} in the salt channels for both tests) throughout the test. This migration can be attributed to the smaller size and higher mobility of protons compared to sodium ions (0.282 nm and 9.31 × 10^{-9} m^2 s^{-1}, respectively). In the specific case of S1_B1_A1, by the end of the test, the concentrations of Na^+ and H^+ became comparable (both ~0.01 mol L^{-1}), as did their apparent transport numbers, when defined as in the work of Filingeri et al. [11]. In scenario S1_B1_A1 at the pilot and laboratory scales, at the end of the tests, saline conductivity dropped below 5 mS cm^{-1}, indicating EDBM's potential for advanced schemes for desalination involving concurrent acid-base production. This finding highlights a potential future shift from traditional acid-base-focused EDBM to paradigms also involving desalination. However, further downstream treatment for pH adjustment and refinement would also be required. Alternative configurations can be tested at the laboratory scale, and the results can be directly extended to larger scales by maintaining the same scale-independent parameters.

3.2. Electrical variables and key performance indicators trends

Regarding the electric variables, Fig. 5a and b present the triplet voltage profiles and Fig. 5c and d the current density profiles over time at both scales. The tests began in potentiostatic mode and switched to galvanostatic mode at 200 A m^{-2}. Electrode potential drops were excluded from the laboratory-scale stack voltages, unlike for the pilot-scale measurements (as their impacts were negligible). In tests with imbalanced volumes, under potentiostatic mode, the current initially rose due to the decreased triplet resistance resulting from the increased

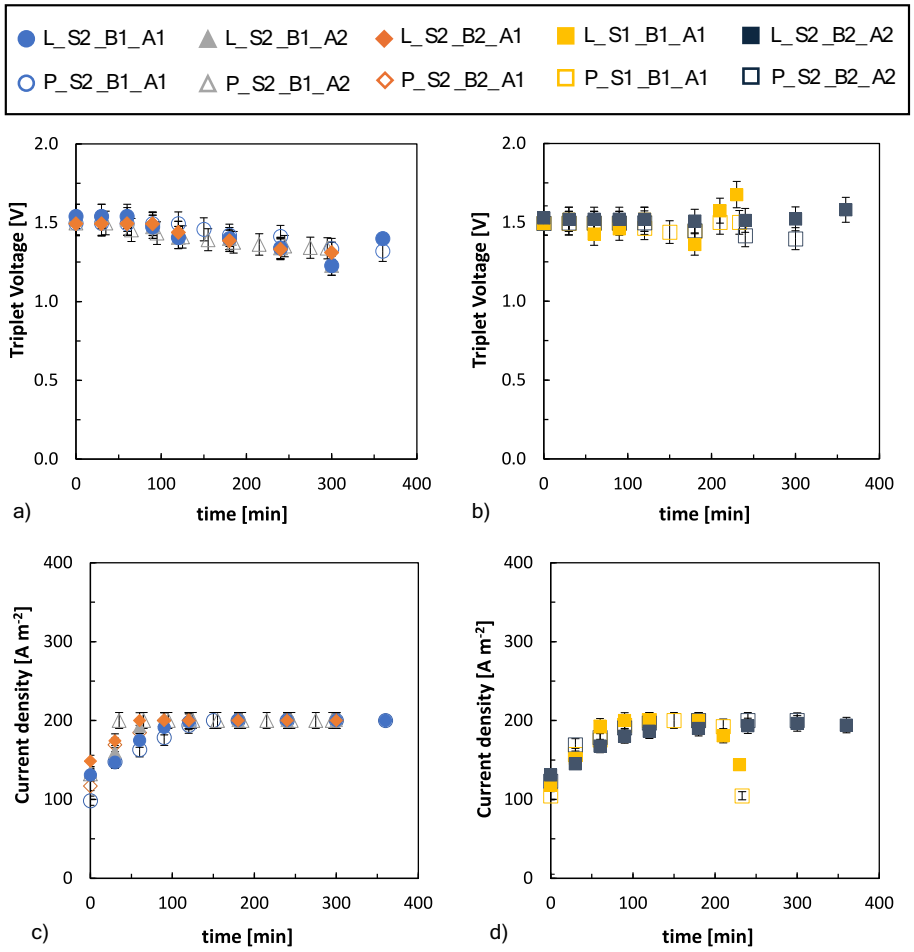

Fig. 5. a) and b) Triplet voltage and c) and d) current density profiles over time for the tests conducted at both pilot and laboratory scales for all the investigated scenarios. a) and c) refer to tests with different initial volumes while b) and d) report tests with the same initial volumes.

acid-base concentrations. This rise was followed by a moderate voltage drop (10–15 %) during the galvanostatic mode at 200 A m^{-2}, as the acid-base channel resistances became negligible compared to the membrane resistances. The tests with balanced volumes showed a similar initial current increase, but at the end of S1_B1_A1, the current decreased and the voltage rose due to increased triplet resistance resulting from the nearly depleted saline conductivity (see Fig. 4b). The results show that, under equivalent operating conditions, the electrical variables exhibit similar behavior at both laboratory and pilot scales.

Overall, the raw data obtained from both systems showed minimal deviations from each other, thus demonstrating the robustness of the process and its consistency upon scale-up.

Particularly, a very good agreement between the operating variables at the laboratory and pilot scales was observed for all the investigated scenarios. The average deviation in salt conductivity, triplet voltage, and current density for all timepoints and across the different scenarios were ~ 2.6 %, ~1.7 %, and ~ 2.6 %, respectively. Conversely, a larger deviation of ~12.9 % was obtained for the proton concentration in the salt solution over time and across the different tests. The larger deviation in the proton concentration is due to the very small values. Table S1 in the Supplementary Material reports the average deviation over time between the lab-scale and the pilot-scale for each scenario and different process variables.

In terms of key performance indicators, Fig. 6 shows the current efficiency (CE) and the Specific Energy Consumption (SEC) across the different operating scenarios at both laboratory- and pilot-scales.

Under equivalent operating conditions, both laboratory-scale and pilot-scale units show similar trends of SEC and current efficiency during the initial phases of the tests. However, it should be noted that as the concentration in the saline compartment approaches zero—towards the end of the tests—even small differences in concentration can lead to significant variations in the main process variables, making direct comparison less meaningful. The results show that current efficiency exhibits a decreasing trend over time, which is approximately linear, primarily due to increased ion crossover and reduced selectivity of ion transport as the concentrations within the compartments increase. The current efficiency ranged from 41 % to 99 % for scenarios where the volumes of acid, base, and salt were imbalanced, while they varied between 47 % and 99 % when the volumes were balanced. In the latter case, at comparable acid/base concentrations achieved, the current efficiency values were similar, thus confirming that the unit's performance is independent of the solution volumes when they are equal at both scales. Indeed, as previously mentioned, when the volumes are changed but kept equal with each other, the only parameter affected is the processing time. The trend in CE over time appears consistent with observations reported in the literature, showing values (47–99 % and 41–99 %) that are comparable to or even higher than those summarized in Table 1, under similar operating conditions (i.e., concentrations up to 1 mol L^{-1}).

Conversely, the SEC tends to increase over time. This rise is primarily attributed to the reduction in current efficiency. Although SEC also depends on voltage, the voltage was constant in the first part of the test and slightly decreased in the second part (see Fig. 5 a and b). A notable difference was observed in test S2_B1_A2, where doubling the acid volume resulted in a 23 % (lab-scale) and 25 % (pilot-scale) lower SEC at the end of the experiment compared to test S2_B1_A1.

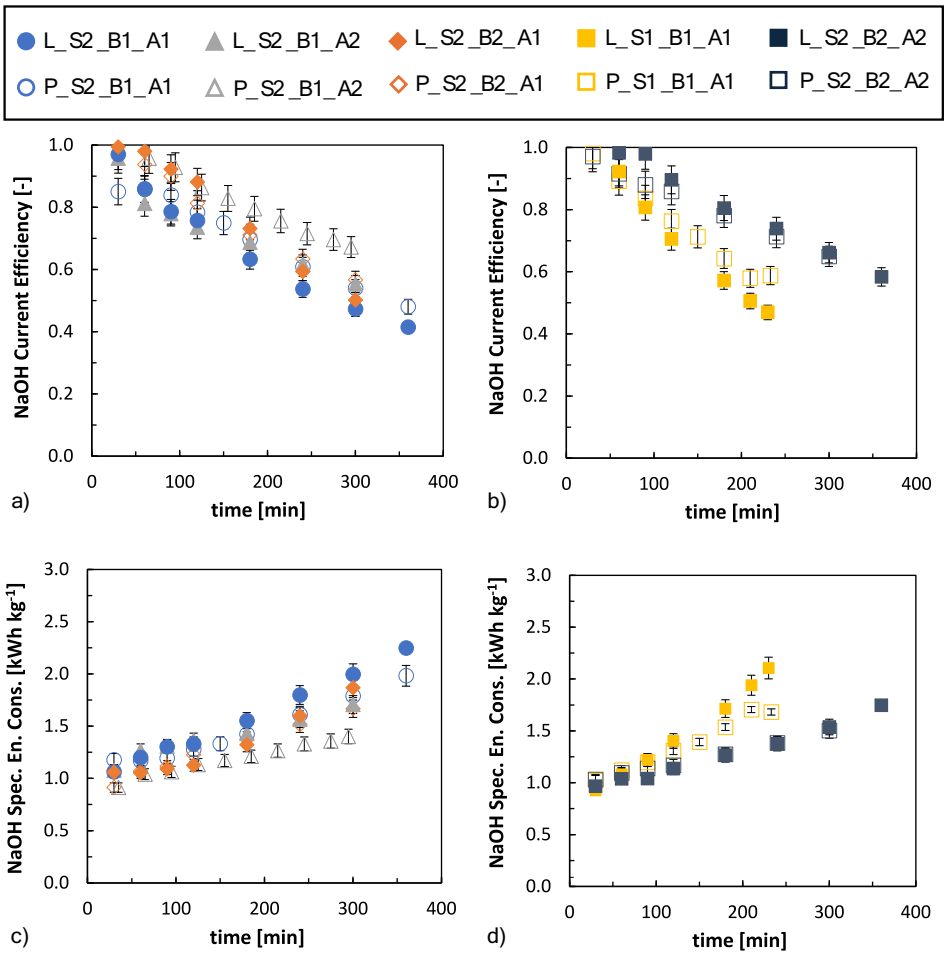

Fig. 6. a) and b) Current efficiency, and c) and d) Specific energy consumption profiles over time for the tests conducted at both pilot and laboratory scales for all the scenarios investigated. a) and c) refer to tests with different initial volumes while b) and d) report tests with the same initial volumes.

Operating at lower acid and base concentrations may be beneficial to maximize productivity and minimize the total installed membrane area, although this would be more useful for applications where diluted solutions can be used in the process, such as the in-situ utilization of acid and base. However, in cases where the low solution concentration is not an issue, practical challenges may still exist, such as increased handling volumes.

It is worth noting that, at the target concentration of 0.5 mol L^{-1} OH^- in the alkaline solution, the average SEC was 1.24 kWh kg $^{-1}_{NaOH}$, regardless of the system scale, while the minimum value (1.05 kWh kg $^{-1}_{NaOH}$) was reached at the pilot scale during the S2_B1_A2 test. These results are comparable to, or even lower than, those reported in the literature under similar conditions (see Table 1). At OH^- concentration of ~1 mol L^{-1}, the SEC was ~2 kWh kg $^{-1}_{NaOH}$ for the S2_B1_A1 test and ~ 1.45 kWh kg $^{-1}_{NaOH}$ for the S2_B1_A2 test. These values are lower than those obtained using Astom Co. membranes at the laboratory scale [28] and Fumatech membranes at the pilot scale [33], as reported in Table 1. Consequently, the use of the alkaline solution as the ERS did not impact the results at either the laboratory or pilot scale. Moreover, this configuration offers the additional advantage of eliminating a fourth hydraulic loop (i.e., that dedicated to the ERS), thereby reducing capital and operating costs compared to the more conventional four-solution design.

The best performance, in terms of lower SEC, was measured when doubling the acid solution volume.

Fig. 7 shows the variation of current efficiency as a function of SEC. Fig. 7 presents an alternative representation of current efficiency and SEC, plotted one as a function of the other. As can be observed, all data points from tests with either unbalanced (Fig. 7a) or equal initial volumes (Fig. 7b) are approximately aligned along the same curve. Interestingly, these experimental points would remain aligned even if all scenarios were plotted together on the same graph (combining graphs a and b).

The observed power-law trend can be explained by combining the definitions of SEC and CE, as detailed in the Supplementary Material. Specifically, CE is inversely proportional to SEC and directly proportional to the applied voltage. As a result, CE can be described by a function of the form K/SEC. The consistent alignment of the curves across different scales suggests that the value of K can be considered constant, thus indicating that these curves are a characteristic feature of the EDBM unit's performance. In other words, SEC and current efficiency can be considered as scale-independent output variables of the EDBM system. Once the channel geometry, membrane type, and current density are fixed, the curve appears to hold independently of the absolute size of the equipment. A further development of this modeling approach would be the derivation of current efficiency vs. SEC curves as a function of the applied current density. Such an approach could support the implementation of automation and control systems for operating the EDBM under optimal conditions.

These results have several practical implications. Firstly, as already mentioned, they demonstrate that performance studies conducted at the laboratory scale are reliably indicative of outcomes at the pilot scale. Consequently, either laboratory-scale experimental data or validated mathematical models from laboratory-scale tests should suffice when designing scaled-up systems.

Multi-scale modeling tools, previously validated at the laboratory

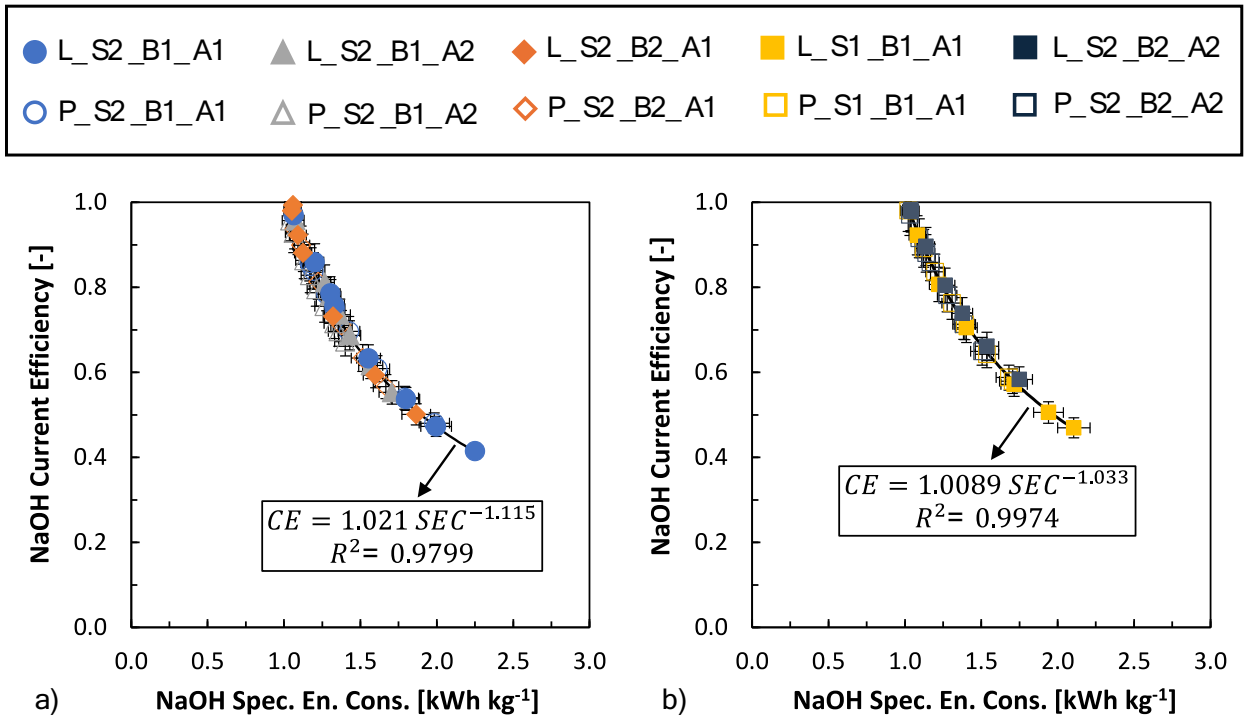

Fig. 7. Current efficiency vs. specific energy consumption referred to NaOH product for the tests conducted at both pilot and laboratory scales for all the scenarios investigated. a) refers to tests with different initial volumes while b) reports tests with the same initial volumes.

scale, are available in the literature. The findings of this work suggest that these tools can be reliably used to design and predict the behavior of larger-scale systems without compromising accuracy or rigor, provided that the upscaled systems operate under the same scale-independent parameters.

Moreover, once validated at the laboratory scale, such mathematical process models can be employed not only for unit simulation but also for the rigorous process optimization of industrial-scale EDBM systems. These simulation tools enable the identification of optimal operating conditions and design features prior to scale-up, thereby reducing experimental efforts and supporting the efficient design of automated and high-performance EDBM units.

3.3. Scale-up technical challenges and cost analysis

Despite the transferability of performance data across unit sizes, additional complexities arise during scale-up for a researcher who is willing to investigate using conventional R&D lab-scale approaches. These challenges are mainly related to the increased size of equipment and treated volumes. At larger scales, designing plant-specific characteristics, such as the hydraulic and electrical circuits, becomes more complex and demanding. For example, corrosion-resistant materials (especially for long-term operations), pressurized equipment, and enhanced safety measures for the application of high DC/AC currents may be required. The continuous monitoring of micro-filter fouling and timely replacement based on pressure-drop evolution are necessary, alongside systematic washing and periodic chemical cleanings to mitigate organic/inorganic fouling. Proper storage protocols are also necessary to help preserve membrane performance. Furthermore, an advanced automation system is essential to manage volume variations due to osmotic and electro-osmotic water transport. Additionally, purge and make-up streams should be used to prevent salt accumulation in the acid and base tanks. Overall, robust sensors, leak-containment measures, and maintenance strategies are crucial to ensure safe and reliable large-scale operations.

From an economic perspective, scale-up also introduces significant cost-related considerations. The capital costs (CAPEX) can mainly be divided into stack and peripherals costs.

The former includes costs related to the membranes, spacers, electrodes (including their possible periodic replacement), and all the components required to assemble the unit (e.g., plates and frames). The latter includes, for example, the costs of pumps and power supplies, advanced automation, and safety systems. In scaled-up systems, specific operational requirements arise, such as the use of corrosion-resistant materials. Similarly, the need for regular maintenance, and micro-filter replacement increases the operational expenditure (OPEX).

Additionally, the effective management of water transport, the purge and make-up streams, and system automation plays a key role in minimizing resource consumption and downtime, thereby enhancing economic profitability. To provide an indicative cost per kilogram of acid and base produced and, thus, offer a tool for economic scale-up, a simplified cost analysis was performed.

The adopted economic model is reported in the Supplementary Material, while the inputs used for the cost analysis are listed in Table 5.

The analyses were conducted under the investigated scenarios described in Section 2.4, namely S2_B1_A2, S2_B2_A1, S2_B1_A1, S1_B1_A1, S2_B2_A2.

Table 5
Input variables ranges of the economic model.

	Units	Value range	Reference value
Capital costs			
AEM and CEM	€ m^{-2}	50–200	100
BPM	€ m^{-2}	150–600	300
Spacer	€ m^{-2}	5–20	10
Electrode	€ m^{-2}	250–1,000	500
Other economic inputs			
Electricity price	€ kWh^{-1}	0.05–0.20	0.10
Membranes lifetime	years	2–10	5
Project lifetime	years	10	10
Discount rate	%	2–10	5

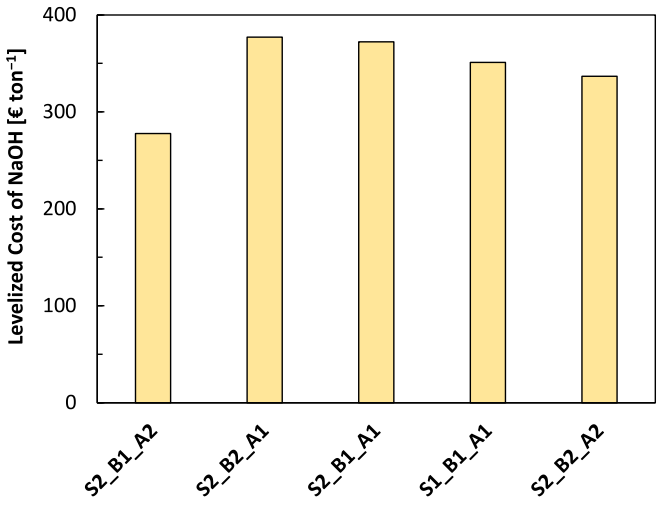

Fig. 8. Levelized cost of NaOH for the five analyzed scenarios: S2_B1_A2, S2_B2_A1, S2_B1_A1, S1_B1_A1, S2_B2_A2.

Fig. 8 shows a histogram with the resulting LCoNaOH values for the five scenarios analyzed referring to the production of NaOH as 0.5 mol L^{-1} OH^- solutions.

Interestingly, the analyzed scenarios resulted in better LCoNaOH outcomes compared to current market prices [49,50]. The lowest levelized cost (~278 € ton^{-1}) and, thus, the most economically favorable outcome, was achieved in scenario S2_B1_A2, which corresponds to the case where the acid concentration is reduced. Starting from the scenario (S2_B1_A2) with the minimum LCoNaOH, a sensitivity analysis was performed using a tornado diagram (Fig. 9) to identify the economic variable that most affects LCoNaOH.

The results shown in Fig. 9a indicate that the LCoNaOH is predominantly driven by the cost of the membrane triplet (i.e., the combined cost of the bipolar membrane and the anionic and cationic monopolar membranes), with relative variations of −79 and + 158 €/ton compared to the baseline of ~278 € ton^{-1}. Variations in the LCoNaOH associated with the spacer and electrode costs were on average < 10 €/ton. While it is intuitive that the spacer cost (ranging between 5 and 20 €/m^2) has a negligible influence on the LCoNaOH, the electrode cost might initially appear to have a major impact (250–1,000 €/m^2). However, the total

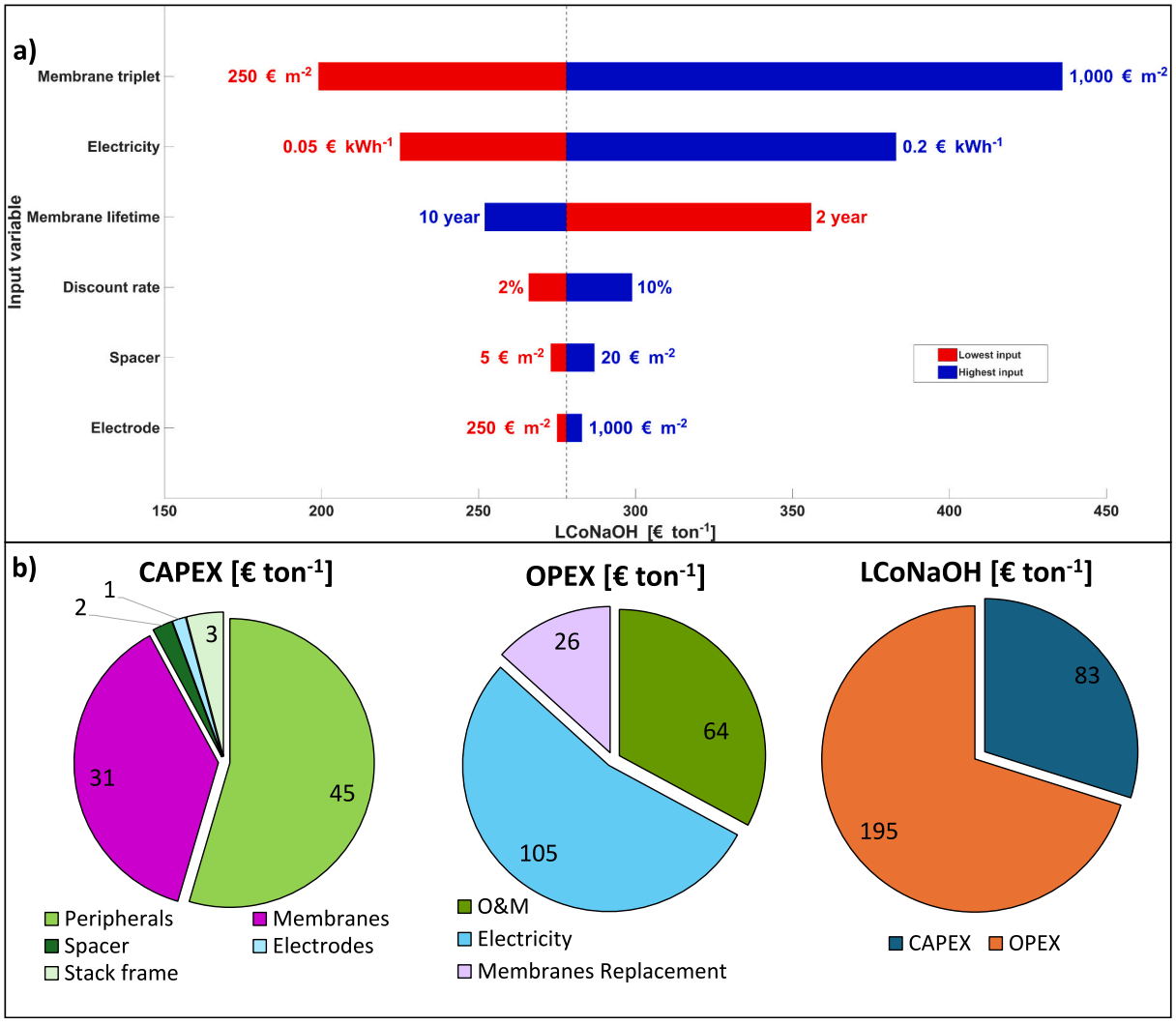

Fig. 9. a) Tornado diagram showing how the LCoNaOH varies with changes in the economic model inputs, namely (from top to bottom): cost of the membrane triplet, membrane lifetime, electricity price, discount rate, spacer cost, and electrode cost. b) Pie charts illustrating, for the base case scenario, the distribution of CAPEX, OPEX, and their respective contributions to the LCoNaOH. The analysis referred to S2_B1_A2 scenario.

installed electrode area corresponds only to the cathodic and anodic sections of the unit and, thus, contributes only marginally to the LCoNaOH at the industrial scale characterized by a high number of triplets. The discount rate, varying between 2 % and 10 %, also showed little effect on the levelized cost. Conversely, the electricity cost played a significant role, as shifting from 5 c€ /kWh to 20 c€ /kWh led to a variation of −52 and + 105 €/ton. Finally, as membrane lifetime also had a notable effect, it is advisable to implement membrane cleaning or scaling removal procedures to limit the stack replacement frequency and, thus, improve system profitability.

Fig. 9b shows the breakdown of the baseline case for the NaOH best performance scenario (S2_B1_A2) in terms of the percentage contribution of each component, CAPEX and OPEX, to the LCoNaOH.

In the analyzed scenario, OPEX represented the dominant share (~70 %) of LCoNaOH, with electricity cost being the main contributor (54 % of OPEX), although maintenance and membrane replacement costs also accounted for a non-negligible portion. Within CAPEX, membranes and peripherals costs were the main components (92 % of CAPEX, corresponding to ~27 % of LCoNaOH). Based on this analysis, a further improvement in the profitability of the EDBM process could be achieved either through the optimization of the membrane manufacturing (particularly of the bipolar membranes) to reach competitive market prices and, thus, reduce CAPEX, or through the use of renewable energy sources, such as solar power, to minimize electricity costs.

4. Conclusions

This study provides a comprehensive evaluation of Electrodialysis with Bipolar Membranes (EDBM) at two different scales, laboratory and semi-industrial. Once identified the main scale-independent parameters, which allowed to select equivalent operating conditions for the two scale plants, results demonstrated that process performance were highly consistent across scales, with average deviations of ~4.7 % in terms of the main monitored variables and performance indicators. These findings support the scalability of the EDBM process and validate the reliability of laboratory-scale data and modeling tools for designing larger-scale systems.

As an application example, the work has demonstrated how the ratio of initial solution volumes plays a more significant role in determining EDBM performance than the absolute volumes. The adoption of an initial volume of acid and salt double than that of the base solution resulted in higher final NaOH concentrations (up to 1.14 mol L^{-1}) and current efficiencies (86 % at 0.5 mol L^{-1} OH^-), lower SEC values (minimum values of 1.18 and 1.24 kWh kg_{NaOH}^{-1} obtained in the S2_B1_A2 and S2_B1_A1 tests, respectively, at the same target concentration of 0.5 mol L^{-1} OH^-), and the lowest LCoNaOH (278 € ton^{-1}). Furthermore, the observed conductivity and pH trends in the salt compartment suggest that EDBM can potentially be applied for desalination purposes, expanding its scope beyond acid and base production. Finally, the derivation of scale-independent correlations between SEC and current efficiency highlights the robustness of the EDBM system and offers a valuable tool for future process optimization. These insights contribute to the advancement of sustainable chemical production technologies and reinforce the role of EDBM as a promising solution for future industrial implementation for the circular resource management and brine valorization. Further optimization of stack design, process control and energy management will be required for the successful transition from pilot- to full-scale applications. Improvements in membrane materials, system manufacturing and renewable energy integration are expected to make the processes more sustainable and economically competitive.

CRediT authorship contribution statement

Andrea Culcasi: Writing – review & editing, Writing – original draft, Visualization, Validation, Supervision, Software, Methodology, Investigation, Formal analysis, Data curation, Conceptualization. **Antonia Filingeri:** Writing – review & editing, Writing – original draft, Visualization, Validation, Supervision, Software, Methodology, Investigation, Formal analysis, Data curation, Conceptualization. **Alessandro Tamburini:** Writing – review & editing, Supervision, Project administration, Funding acquisition. **Giorgio Micale:** Writing – review & editing, Supervision, Funding acquisition, Formal analysis. **Andrea Cipollina:** Writing – review & editing, Supervision, Resources, Project administration, Methodology, Funding acquisition, Conceptualization.

Declaration of competing interest

The authors declare that they have no known competing financial interests or personal relationships that could have appeared to influence the work reported in this paper.

Acknowledgements

This work was supported by the EU within SEArcularMINE (Circular Processing of Seawater Brines from Saltworks for Recovery of Valuable Raw Materials) project – Horizon 2020 programme, Grant Agreement No. 869467. This output reflects only the author's view. The European Health and Digital Executive Agency (HaDEA) and the European Commission cannot be held responsible for any use that may be made of the information contained therein.

This work was also supported by the project funded under the National Recovery and Resilience Plan (NRRP), Mission 4 Component 2 Investment 1.3 - Call for tender No. 1561 of 11.10.2022 of Ministero dell'Università e della Ricerca (MUR); funded by the European Union – NextGenerationEU. Award Number: Project code PE0000021, Concession Decree No. 1561 of 11.10.2022 adopted by Ministero dell'Università e della Ricerca (MUR), CUP – B73C22001280006, Project title “Network 4 Energy Sustainable Transition – NEST”.

Appendix A. Supplementary data

Supplementary data to this article can be found online at https://doi.org/10.1016/j.cej.2025.172374.

Data availability

Data will be made available on request.

References

[1] G.A. Blengini, C.E.L. Latunussa, U. Eynard, C. Torres de Matos, D. Wittmer, K. Georgitzikis, C. Pavel, S. Carrara, L. Mancini, M. Unguru, D. Blagoeva, F. Mathieux, D. Pennington, Study on the EU's List of Critical Raw Materials (2020) Final Report, 2020, https://doi.org/10.2873/904613.

[2] Ullmann's Encyclopedia of Industrial Chemistry, Wiley, 2000, https://doi.org/10.1002/14356007.

[3] P. Lerch, F. Scheller, D.G. Reichelt, K. Menzel, T. Bruckner, Electricity cost and CO2 savings potential for chlor-alkali electrolysis plants: benefits of electricity price dependent demand response, Appl. Energy 355 (2024), https://doi.org/10.1016/j.apenergy.2023.122263.

[4] R.R. Contreras, J. Almarza, L. Rincón, C. Ruiz, Green sodium hydroxide for industrial purposes. A short review, J. Environ. Chem. Eng. 13 (2025), https://doi.org/10.1016/j.jece.2024.114972.

[5] H. Wang, Y. Wang, J. Yan, R. Fu, B. Wang, C. Jiang, Y. Wang, T. Xu, Bipolar membrane electrodialysis: a promising paradigm for caustic soda production, AICHE J. 70 (2024), https://doi.org/10.1002/aic.18260.

[6] T. Chen, J. Bi, Z. Ji, J. Yuan, Y. Zhao, Application of bipolar membrane electrodialysis for simultaneous recovery of high-value acid/alkali from saline wastewater: an in-depth review, Water Res. 226 (2022), https://doi.org/10.1016/j.watres.2022.119274.

[7] X. Zhou, X. Li, D. Yang, X. Jing, W. Yan, H. Xu, Bipolar membranes: a review on principles, preparation methods and applications in environmental and resource recovery, Chem. Eng. J. 507 (2025), https://doi.org/10.1016/j.cej.2025.160184.

[9] M. Herrero-Gonzalez, N. Admon, A. Dominguez-Ramos, R. Ibañez, A. Wolfson, A. Irabien, Environmental sustainability assessment of seawater reverse osmosis brine valorization by means of electrodialysis with bipolar membranes, Environ.

Sci. Pollut. Res. 27 (2020) 1256–1266, https://doi.org/10.1007/s11356-019-04788-w.
[10] R. Pärnamäe, S. Mareev, V. Nikonenko, S. Melnikov, N. Sheldeshov, V. Zabolotskii, H.V.M. Hamelers, M. Tedesco, Bipolar membranes: a review on principles, latest developments, and applications, J. Membr. Sci. 617 (2021) 118538, https://doi.org/10.1016/j.memsci.2020.118538.
[11] A. Filingeri, J. Lopez, A. Culcasi, T. Leon, A. Tamburini, J. Luis Cortina, G. Micale, A. Cipollina, In-depth insights on multi-ionic transport in electrodialysis with bipolar membrane systems, Chem. Eng. J. 468 (2023), https://doi.org/10.1016/j.cej.2023.143673.
[12] A. Culcasi, L. Gurreri, A. Cipollina, A. Tamburini, G. Micale, A comprehensive multi-scale model for bipolar membrane electrodialysis (BMED), Chem. Eng. J. 437 (2022), https://doi.org/10.1016/j.cej.2022.135317.
[13] A. Culcasi, L. Gurreri, A. Tamburini, A. Cipollina, I.D.L. Bogle, G. Micale, Improving efficiency and discharge power of acid-base flow battery via a bi-objective optimisation, J. Energy Storage 66 (2023), https://doi.org/10.1016/j.est.2023.107429.
[15] J. López, A. Culcasi, M. Fernández de Labastida, A. Tamburini, G. Micale, A. Cipollina, J.L. Cortina, Integration of nanofiltration, ion exchange, and electrodialysis with bipolar membranes for the valorisation of brines: from seawater desalination plants to on-site chemicals production facilities, J. Environ. Manag. 381 (2025), https://doi.org/10.1016/j.jenvman.2025.125119.
[16] G. Virruso, C. Cassaro, F. Vassallo, A. Filingeri, A. Pellegrino, A. Tamburini, A. Cipollina, G.D.M. Micale, A pilot plant investigation on a real seawater brine valorisation via electrodialysis with bipolar membranes, J. Water Process Eng. 69 (2025), https://doi.org/10.1016/j.jwpe.2024.106741.
[17] J. Lopez, A. Filingeri, A. Culcasi, M. Fernández de Labastida, A. Tamburini, J. L. Cortina, G. Micale, A. Cipollina, Electrodialysis with bipolar membranes to valorise saline waste streams: Analysing the fate of valuable minor elements, Sci. Total Environ. 958 (2025), https://doi.org/10.1016/j.scitotenv.2024.177934.
[18] D. Ankoliya, A. Mudgal, M.K. Sinha, P. Davies, K. Park, R.R. Alegre, V. Patel, J. Patel, Techno-economic analysis of integrated bipolar membrane electrodialysis and batch reverse osmosis for water and chemical recovery from dairy wastewater, J. Clean. Prod. 420 (2023), https://doi.org/10.1016/j.jclepro.2023.138264.
[19] N. Adiba, X. Wang, C. Chang, X. Xu, Y. Liu, C. Ji, Q. Wang, Y. Ren, J. Wang, Z. Liu, Z. Ma, J. Gao, Multi-stage membrane integrated system to achieving low-mixed-salt-discharge of high-salinity mining wastewater: system design and experimental validation, Chem. Eng. Res. Des. 202 (2024) 12–22, https://doi.org/10.1016/j.cherd.2023.12.015.
[20] M. Adigüzel, J. Erkmen, M.T. Yilmaz, Application and optimization of bipolar membrane process for drinking water production from Black Sea, J. Clean. Prod. 408 (2023), https://doi.org/10.1016/j.jclepro.2023.136814.
[21] J. Mustafa, N. Ghasem, M.H. El-Naas, B. Van der Bruggen, A.H. Al-Marzouqi, Synergistic approach for carbon dioxide capture and reject brine treatment: integrating selective electrodialysis and bipolar membrane electrodialysis, J. Clean. Prod. 438 (2024), https://doi.org/10.1016/j.jclepro.2024.140578.
[22] A. Hussain, H. Wang, R. Fu, N.U. Afsar, B. Wang, C. Jiang, Y. Wang, T. Xu, Ion transport behavior in bipolar membrane Electrodialysis: role of anions, Ind. Eng. Chem. Res. 62 (2023) 698–707, https://doi.org/10.1021/acs.iecr.2c03812.
[23] M. Herrero-Gonzalez, P. Diaz-Guridi, A. Dominguez-Ramos, A. Irabien, R. Ibañez, Highly concentrated HCl and NaOH from brines using electrodialysis with bipolar membranes, Sep. Purif. Technol. 242 (2020) 116785, https://doi.org/10.1016/j.seppur.2020.116785.
[24] C. Du, J.R. Du, X. Zhao, F. Cheng, M.E.A. Ali, X. Feng, Treatment of brackish water RO brine via bipolar membrane Electrodialysis, Ind. Eng. Chem. Res. 60 (2021) 3115–3129, https://doi.org/10.1021/acs.iecr.1c00370.
[25] K. Song, S.C. Chae, J.H. Bang, Separation of sodium hydroxide from post-carbonation brines by bipolar membrane electrodialysis (BMED), Chem. Eng. J. 423 (2021), https://doi.org/10.1016/j.cej.2021.130179.
[26] A. Filingeri, M. Herrero-Gonzalez, J. O'Sullivan, J.L. Rodriguez, A. Culcasi, A. Tamburini, A. Cipollina, R. Ibañez, M.C. Ferrari, J.L. Cortina, G. Micale, Acid/base production via bipolar membrane Electrodialysis: brine feed streams to reduce fresh water consumption, Ind. Eng. Chem. Res. 63 (2024) 3198–3210, https://doi.org/10.1021/acs.iecr.3c03553.
[27] A. Lugo, M.F. Ahmed, T.L. Oddonetto, P.S. Senanayake, I. Basnayake, Z. Stoll, M. Ehsani, N.E. Moe, J. Barber, H. Wang, P. Xu, Operational optimization of bipolar membrane electrodialysis for acid and base production in zero liquid discharge of high-salinity brine, Desalination 615 (2025), https://doi.org/10.1016/j.desal.2025.119290.
[28] D. Yang, H. Liu, Z.H. Foo, Q. She, The critical role of monopolar ion exchange membrane properties in ion transport and acid-base production in bipolar membrane electrodialysis, Desalination 615 (2025), https://doi.org/10.1016/j.desal.2025.119306.
[29] H. Ruan, S. Wu, X. Chen, J. Zou, J. Liao, H. Cui, Y. Dong, Y. Qiu, J. Shen, Capturing CO2 with NaOH solution from reject brine via an integrated technology based on bipolar membrane electrodialysis and hollow fiber membrane contactor, Chem. Eng. J. 450 (2022), https://doi.org/10.1016/j.cej.2022.138095.
[30] K. Song, S.C. Chae, J.H. Bang, Separation of sodium hydroxide from post-carbonation brines by bipolar membrane electrodialysis (BMED), Chem. Eng. J. 423 (2021), https://doi.org/10.1016/j.cej.2021.130179.
[31] A. Filingeri, A. Culcasi, M. Nanfara, C. Cassaro, A. Tamburini, G. Micale, A. Cipollina, Exploring differential pressure-induced hydraulic flows in pilot-scale Electrodialysis with bipolar membranes, J. Environ. Manag. 373 (2025), https://doi.org/10.1016/j.jenvman.2024.123538.
[32] J.W. Qin, S. Tang, J.L. Shi, T.F. Zhang, L. Yang, F. Wang, L. Yin, Y.F. Zhuang, Bipolar membrane electrodialysis for producing acid and alkali from concentrated seawater: industrial application in Bohai Sea, China, J. Water Process Eng. 76 (2025), https://doi.org/10.1016/j.jwpe.2025.108266.
[33] C. Cassaro, G. Virruso, A. Culcasi, A. Cipollina, A. Tamburini, G. Micale, Electrodialysis with bipolar membranes for the sustainable production of chemicals from seawater brines at pilot plant scale, ACS Sustain. Chem. Eng. 11 (2023) 2989–3000, https://doi.org/10.1021/acssuschemeng.2c06636.
[34] D. Pintossi, C. Simões, M. Saakes, Z. Borneman, K. Nijmeijer, Predicting reverse electrodialysis performance in the presence of divalent ions for renewable energy generation, Energy Convers. Manag. 243 (2021), https://doi.org/10.1016/j.enconman.2021.114369.
[35] R. Fu, H. Wang, J. Yan, R. Li, B. Wang, C. Jiang, Y. Wang, T. Xu, A cost-effective and high-efficiency online ED-BMED integrated system enables the conversion of 3.5 wt% NaCl aqueous solution into 6.20 Mol/L NaOH, Chem. Eng. Sci. 270 (2023), https://doi.org/10.1016/j.ces.2023.118523.
[36] H.R. Yang, B. Li, C.Q. Zhang, J.C. Yang, Y.M. Zheng, M. Younas, Y.H. Jiang, Z. H. Yuan, Bipolar membrane electrodialysis for sustainable utilization of inorganic salts from the reverse osmosis concentration of real landfill leachate, Sep. Purif. Technol. 308 (2023), https://doi.org/10.1016/j.seppur.2022.122898.
[37] F. Ferella, A. Suichies, B.A. Abdelkader, N.K. Dabhi, J. Werber, C.F. de Lannoy, Ocean alkalinity enhancement using bipolar membrane Electrodialysis: technical analysis and cost breakdown of a full-scale plant, Ind. Eng. Chem. Res. (2025), https://doi.org/10.1021/acs.iecr.4c04364.
[38] A. Hussain, H. Yan, N. Ul Afsar, C. Jiang, Y. Wang, T. Xu, Multistage-batch bipolar membrane electrodialysis for base production from high-salinity wastewater, Front. Chem. Sci. Eng. 16 (2022) 764–773, https://doi.org/10.1007/s11705-021-2114-2.
[39] H. Tang, X. Wang, X. Zhao, Y. Dong, B. Xu, L. Wang, Ion migration characteristics during the bipolar membrane electrodialysis treatment of concentrated reverse osmosis brine, Desalination 561 (2023), https://doi.org/10.1016/j.desal.2023.116660.
[40] S. Wu, R. Fu, J. Yan, H. Wang, B. Wang, Y. Wang, T. Xu, Online neutralization promotes water dissociation equilibrium forward in bipolar membranes to achieve 9.2 Mol/L NaOH production, Chem. Eng. J. 490 (2024), https://doi.org/10.1016/j.cej.2024.151610.
[41] O. Scialdone, C. Guarisco, S. Grispo, A.D. Angelo, A. Galia, Investigation of electrode material - redox couple systems for reverse electrodialysis processes. Part I: Iron redox couples, J. Electroanal. Chem. 681 (2012) 66–75, https://doi.org/10.1016/j.jelechem.2012.05.017.
[42] A. Filingeri, M. Philibert, E. Filloux, A. Brehant, A. Tamburini, A. Cipollina, G. Micale, Assisted-reverse Electrodialysis for permeate remineralization from surface water RO brines: experimental investigation with multi-ionic solutions, J. Water Process Eng. 67 (2024), https://doi.org/10.1016/j.jwpe.2024.106156.
[43] G. Hopsort, Q. Cacciuttolo, D. Pasquier, Electrodialysis as a key operating unit in chemical processes: from lab to pilot scale of latest breakthroughs, Chem. Eng. J. 494 (2024), https://doi.org/10.1016/j.cej.2024.153111.
[44] A. Pellegrino, A. Culcasi, A. Cosenza, A. Cipollina, A. Tamburini, G. Micale, Reducing parasitic currents in acid-base flow batteries by decreasing the manifold cross-sectional area: experiments and modelling, Chem. Eng. Sci. 299 (2024), https://doi.org/10.1016/j.ces.2024.120438.
[45] A. Culcasi, L. Gurreri, A. Zaffora, A. Cosenza, A. Tamburini, A. Cipollina, G. Micale, Ionic shortcut currents via manifolds in reverse electrodialysis stacks, Desalination 485 (2020), https://doi.org/10.1016/j.desal.2020.114450.
[46] G. Kim, H. Kim, M. Kim, N. Kim, B. Lee, S. Kim, X. Su, C. Kim, Scale-up strategies for redox-mediated Electrodialysis for desalination: the role of electrode and channel stacks, ChemSusChem 18 (2025), https://doi.org/10.1002/cssc.202500452.
[47] S. Skogestad, Simple Analytic Rules for Model Reduction and PID Controller Tuning §, n.d. www.elsevier.com/locate/jprocont.
[48] P.S. Fruehauf'a, I.-L. Chien, M.D. Lauritsen, Simplified IMC-PID Tuning Rules, 1994.
[49] E. Medina-Martos, J.L. Gálvez-Martos, J. Almarza, C. Lirio, D. Iribarren, A. Valente, J. Dufour, Environmental and economic performance of carbon capture with sodium hydroxide, J. CO_2 Util. 60 (2022), https://doi.org/10.1016/j.jcou.2022.101991.
[50] Y. Cao, M. Kasaeian, H. Abbasspoor, M. Shamoushaki, M.A. Ehyaei, S. Abanades, Energy, exergy, and economic analyses of a novel biomass-based multigeneration system integrated with multi-effect distillation, electrodialysis, and LNG tank, Desalination 526 (2022), https://doi.org/10.1016/j.desal.2022.115550.